Journal of Colloid and Interface Science 453 (2015) 260–269

Contents lists available at ScienceDirect

Journal of Colloid and Interface Science

www.elsevier.com/locate/jcis

Hantzsch dihydropyridines: Privileged structures for the formation of well-defined gold nanostars

Claudio Zapata-Urzúa [a,1], Magdalena Pérez-Ortiz [a,1], Gerardo A. Acosta [c], Joan Mendoza [h], Lluis Yedra [h], Sonia Estradé [h], Alejandro Álvarez-Lueje [a], Luis J. Núñez-Vergara [a,2], Fernando Albericio [c,d,e,f,*], Rodolfo Lavilla [g,*], Marcelo J. Kogan [a,b,*]

[a] Faculty of Chemical and Pharmaceutical Sciences, University of Chile, Sergio Livingstone 1007, Independencia, Santiago, Chile
[b] Advanced Center for Chronic Diseases (ACCDiS), Chile
[c] Institute for Research in Biomedicine and CIBER-BBN, Barcelona Science Park, Baldiri Reixac 10, 08028 Barcelona, Spain
[d] Department of Organic Chemistry, University of Barcelona, Martí i Franquès 1, 08028 Barcelona, Spain
[e] Yachay Tech School of Chemistry and Chemical Engineering Yachay City of Knowledge Urcuqui-100199, Ecuador
[f] School of Chemistry and Physics, University of KwaZulu-Natal, 4001 Durban, South Africa
[g] Laboratory of Organic Chemistry, Faculty of Pharmacy, University of Barcelona, Avda Joan XXII s/n, 08028 Barcelona, Spain
[h] Scientific and Technological Centres, University of Barcelona, Lluís Solé I Sabarís 1, 08028 Barcelona, Spain

GRAPHICAL ABSTRACT

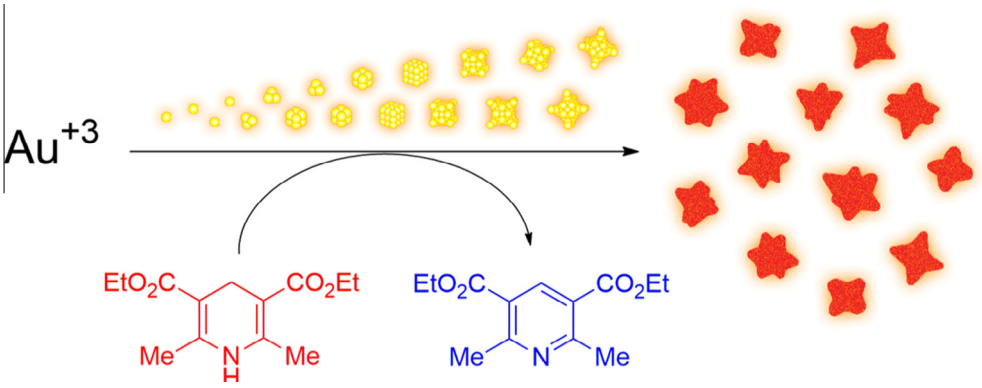

ARTICLE INFO

Article history:
Received 17 November 2014
Accepted 24 April 2015
Available online 1 May 2015

ABSTRACT

Anisotropic and branched gold nanoparticles have great potential in optical, chemical and biomedical applications. However their syntheses involve multi-step protocols and the use of cytotoxic agents. Here, we report a novel one-step method for the preparation of gold nanostructures using only Hantzsch 1,4-dihydropyridines as mild reducing agents. The substituent pattern of the dihydropyridine

Abbreviations: AuNP, Gold nanoparticle; DHP, 2,6-Dimethyl-3,5-diethoxycarbonyl-1,4 dihydropyridine; Ph-DHP, 4-Phenyl-2,6-dimethyl-3,5-diethoxycarbonyl-1,4 dihydropyridine; N-DHP, 1-Benzyl-1,4-Dihydronicotinamide; Pyr, 2,6-Dimethyl-3,5 diethoxycarbonylpyridine; LMW, low molecular weight peptide; HMW, high molecular weight peptide.

* Corresponding authors at: Institute for Research in Biomedicine and CIBER-BBN, Barcelona Science Park, Baldiri Reixac 10, 08028 Barcelona, Spain (F. Albericio). Laboratory of Organic Chemistry, Faculty of Pharmacy, University of Barcelona, Avda Joan XXII s/n, 08028 Barcelona, Spain (R. Lavilla). Faculty of Chemical and Pharmaceutical Sciences, University of Chile, Sergio Livingstone 1007, Independencia, Santiago, Chile (M.J. Kogan).
E-mail addresses: albericio@irbbarcelona.org (F. Albericio), rlavilla@pcb.ub.es (R. Lavilla), mkogan@ciq.uchile.cl (M.J. Kogan).

[1] These authors contributed equally.
[2] Deceased on October 25, 2013.

http://dx.doi.org/10.1016/j.jcis.2015.04.050

This paper is dedicated to the memory of our dear friend Professor Luis J. Núñez-Vergara, a great person and researcher, who made of the fairness, the respect and the friendship his philosophy of life.

Keywords:
Dihydropyridines
Electron microscopy
Gold nanostructures
Nanoparticle synthesis
Nanostars

nucleus was closely related to the ease of formation, morphology and stability of the nanoparticles. We observed nanostructures such as spheres, rods, triangles, pentagons, hexagons, flowers, stars and amorphous. We focused mainly on the synthesis and characterization of well-defined gold nanostars, which were produced quickly at room temperature (25 °C) in high yield and homogeneity. These nanostars presented an average size of 68 nm with mostly four or six tips. Based on our findings, we propose that the growth of the nanostars occurs in the (1 1 1) lattice plane due to a preferential deposition of the gold atoms in the early stages of particle formation. Furthermore, the nanostars were easily modified with peptides remaining stable for more than six months in their colloidal state and showing a better stability than unmodified nanostars in different conditions. We report a new approach using dihydropyridines for the straightforward synthesis of gold nanostructures with controlled shape, feasible for use in future applications.

1. Introduction

Gold nanoparticles (AuNPs) have fascinating optical, electronic, chemical and biological properties and thus are promising for chemical and biomedical applications [1–3]. In this regard, anisotropic and branched AuNPs (multi-pods, star-like, flower-like, urchin-like, among others) are of great interest because of their unique and fine-tuned properties which differ markedly from or are more pronounced than those observed for spherical AuNPs [4], as occurs with the Surface Enhanced Raman Spectroscopy (SERS) effect [5,6] and Near Infrared (NIR) absorption [7,8]. Therefore, branched AuNPs are ideal structures for cutting-edge applications in catalysis [9,10], optical sensing [11], biomedical labeling [12], cancer treatment [13], and as antibacterial agents [14]. A variety of reducing agents, capping agents, stabilizers, surfactants and growth-direction agents have been studied for use in the synthesis of anisotropic and branched AuNPs [15–22]. In many cases the preparation of these particles involves multi-step protocols with low yields, obtaining nanostructures difficult to functionalize [23–27], wherein the characteristics of the synthesis agents and conditions are critical for the formation, stabilization, final morphology and biocompatibility of the nanoparticles [28–31]. In this sense, the most popular methods for the synthesis of anisotropic nanoparticles in high yield are several-step protocols based on seed-mediated approaches using the cationic surfactant cetyltrimethylammonium bromide (CTAB), which is a well-known highly cytotoxic compound [32]. However, in recent years some authors have reported easier synthesis for the preparation of anisotropic gold nanoparticles in high yield, based on one-pot protocols, new mild reduction agents and/or green-chemistry methods free of toxic agents or pure organic solvents [16,33–36].

Furthermore, the Hantzsch 1,4-dihydropyridines, which are important pharmacological agents, have interesting redox properties and can be considered biomimetic reducing agents because of their structural similarity to NADH coenzyme [37–42]. In this regard, the electron transfer displayed by the dihydropyridines is strongly influenced by their substituent patterns [38–41]. Despite their well-known reducing properties, little attention has been devoted to the application of these molecules for the reduction of metallic ions and the growth of metallic nanoparticles [43,44]. Here, we report a novel one-step and surfactant-free synthesis for the preparation of gold nanostructures at 25 °C using only dihydropyridines as reducing agents of the tetrachloroauric acid (Fig. 1a). Studying different dihydropyridines and experimental conditions, we obtained nanostructures of several shapes and sizes. Given the interesting properties of the anisotropic AuNPs and the importance of their preparation in high yield and homogeneity, we focused mainly on the synthesis of well defined star-like AuNPs,

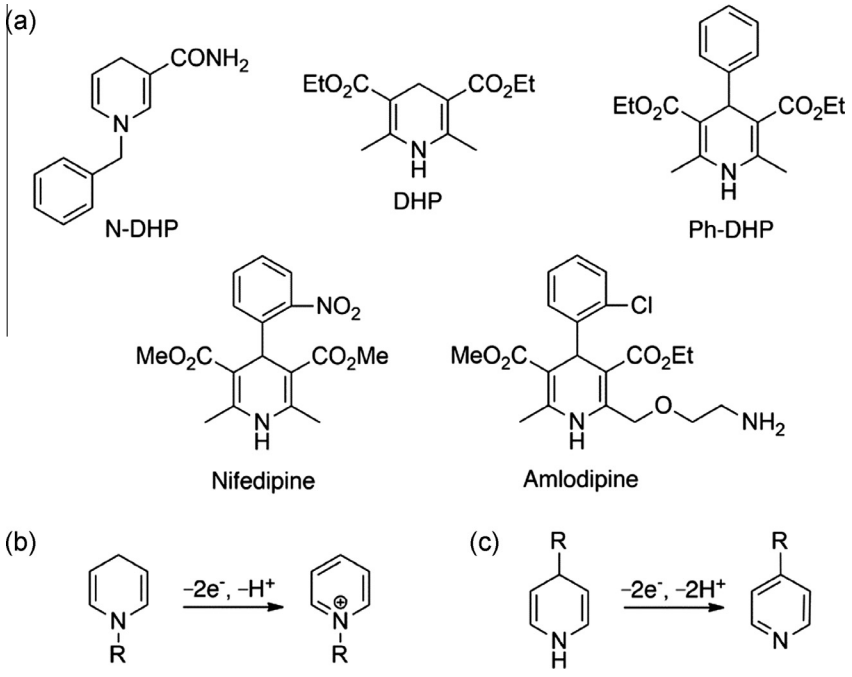

Fig. 1. (a) Chemical structures of the dihydropyridines assayed in the synthesis of gold nanostructures. Representative oxidation scheme of (b) N-substituted and (c) 4-substituted derivatives.

their characterization, structural features and stabilization with biomolecules for potential chemical and biological applications.

2. Experimental section

2.1. Materials

The following reagents were purchased commercially in the higher quality available and were used without further purification: tetrachloroauric (III) acid trihydrate, 2,6-dimethyl-3,5-die thoxycarbonyl-1,4-dihydropyridine (DHP), 2,6-dimethyl-3,5-die thoxycarbonylpyridine (Pyr), nifedipine and amlodipine besylate were purchased from Sigma–Aldrich, while dimethylformamide (DMF) was acquired from SDS and Panreac. The compounds 4-phenyl-2,6-dimethyl-3,5-diethoxycarbonyl-1,4-dihydropyridine (Ph-DHP) and 1-benzyl-1,4-dihydronicotinamide (N-DHP) were synthesized in our laboratory according to previous reports [39,42]. The two peptides assayed for the stabilization and functionalization of the AuNPs, one of low molecular weight (LMW, 739 Da) and the other of high molecular weight (HMW, 3586 Da), were synthesized manually on H-Rink Amide ChemMatrix resin (0.52 mmol/g) using a Fmoc/tert-butyl protection strategy and HBTU, HOBT, DIEA mixture as coupling reagents in DMF, and were characterized by mass spectrometry MALDI-TOF [3]. The chemical structure of the peptides is shown in Fig. S1. Ultrapure Millipore water was used in all experiments.

2.2. Synthesis of gold nanostructures

Due to the low solubility of the dihydropyridines, DMF at 20% was used as cosolvent for the synthesis of gold particles by using the DHP, Ph-DHP, nifedipine and amlodipine derivatives, and at 1% in the case of N-DHP. The syntheses were performed in a water bath at 25 °C (or 60 °C) by using a magnetic stirring with temperature control. In a typical synthesis of the AuNPs, an adequate volume of a fresh solution of each dihydropyridine in DMF (25 mM) was added to a round bottom flask containing a mixture of water (17.5 mL) and DMF (5.0 mL), in order to have final dihydropyridine:Au^{+3} ratios of 1.5:1 and 2.5:1. After homogenization by magnetic stirring, an aqueous solution of $HAuCl_4$ (1 mM, 2.5 mL) was added quickly to the reaction medium with constant stirring. The AuNPs formation was evidenced by characteristic color changes over the time.

2.3. Gold analysis

To evaluate the total conversion of Au^{+3} to gold nanostars, the gold content was determined by neutron activation analysis. The gold colloidal samples were centrifugated at 13,000 rpm for 10 min and the pellet obtained was resuspended in water. This process was repeated three times to ensure the complete remotion of any residual unreduced gold. Later, the colloid samples and the $HAuCl_4$ solution were lyophilized and encapsulated in aluminium foils for the analysis. The samples were irradiated for 30 min in the nuclear reactor, with a thermic neutronic flux around of 7.2×1012 n $\times$ $cm^{-2} \times s^{-1}$. After irradiation the samples were analyzed for 3 min by using a system of high-resolution gamma spectrometry, which was equipped with a hyperpure Ge detector of 10% relative efficiency and resolution of 1.8 keV for the 60Co photopeak of 1333 keV, a multichannel module DSA 2000-A, and an ORTEC pulse generator.

2.4. Nanostructures characterization

The AuNPs synthesized were studied by spectrophotometry, scanning electron microscopy (SEM), transmission electron microscopy (TEM), scanning transmission electron microscopy (STEM), high resolution transmission electron microscopy (HR-TEM) and atomic force microscopy (AFM).

UV–vis spectra were recorded using Shimadzu and Agilent spectrophotometers. Measurements were made by taking a sample of the reaction medium without dilution. SEM images were obtained using a Nova Nano SEM X30 instrument. The samples were prepared depositing a small drop of the colloidal dispersion on a conductive silicon wafer, drying in vacuum at 30 °C for 2 days.

TEM images were obtained with a JEOL JEM-1010 transmission electron microscope operating at 80 kV. All samples were prepared depositing a small drop of the AuNPs on formvar-coated copper-grids, drying completely in air and finally in vacuum at 30 °C for 2 days.

Tomographic 3D reconstructions were performed with a JEOL JEM-2010F transmission electron microscope in scanning mode (STEM), using the high angle annular dark field detector (HAADF). The samples were prepared according to described for TEM analysis but using a holey-carbon film supported by copper-grids. Before analysis the grids were dissected in two. Several images of the same particles were collected by tilting the sample holder from −60° to +60°, every 2°. Finally, the images were aligned and reconstructed using Inspect 3D software.

HR-TEM and the selected area electron diffraction (SAED) analysis were obtained with a JEOL JEM-2100 transmission electron microscope operating at 200 kV. The samples were prepared according to described for the 3D tomography without cutting the grid. Several SAED analyses were carried out on single nanoparticles observed in HR-TEM and the crystal d-spacing values were calculated by measuring the distance between the opposite spots on the same circumference of the diffraction pattern with DigitalMicrograph software.

The samples for AFM were prepared depositing a small drop of the AuNPs on a freshly cleaved mica surface and after some minutes the liquid was rinsing with a nitrogen stream. Samples were analyzed in air at room temperature with a Bruker SNL-10 probe (nominal spring constant: 0.35 nN/nm). AFM Image processing was performed by Research Nanoscope software.

Dynamic light scattering (DLS) analysis were performed at 25 °C by using a Malvern Zetasizer Nano ZS operating at a light source wavelength of 532 nm and with a fixed scattering angle of 90°. Measurements were made by taking 1 mL of the colloidal sample and putting it in a cell with an optical path of 1 cm. To determine the size distribution of the samples, the results were analyzed from the intensity distribution values by using the cumulants method [45]. Six independent samples were analyzed and the maximum intensity of each measurement was registered. The average size and SD were determinate from these six values.

2.5. Electrochemical oxidation potential of dihydropyridines

The dihydropyridine derivatives were studied by differential pulse voltammetry to determinate their electrochemical oxidation potential. The analyses were performed with a CH Instrument electrochemical workstation model CHI650E assembly by using a three-electrode system: glassy carbon (working), platinum wire (auxiliary) and $Ag/AgCl_{sat}$ (reference). The surface of the working electrode was polished with alumina powder (0.3 and 0.05 μm) before each measurement. All dihydropyridines were analyzed at 1 mM into a mixture of DMF/water containing 0.1 M KCl.

2.6. Functionalization of gold nanostars

Considering the isoelectric point of both peptides (6.1 for LMW and 7.2 for HMW), the colloidal solution of star-like AuNPs was adjusted to pH 9-10 with diluted NaOH previous conjugation.

The conjugation and stabilization was performed by adding 50 μL of a fresh solution of each peptide (1 mg/mL) to 10 mL of colloidal solution.

2.7. Stability of gold nanostars

The colloidal stability of the unfunctionalized and functionalized gold nanostars was evaluated spectrophotometrically in different conditions for 48 h at room temperature. Absorption spectra were recorded before and after that the samples were centrifugated (at 13,000 rpm for 10 min) and resuspended in different media: phosphate buffer saline pH 7.4 (PBS), 0.9% NaCl (saline solution), 0.1 M HCl and 0.1 M NaOH.

3. Results and discussion

Several dihydropyridines were studied for their use in the direct preparation of AuNPs from $HAuCl_4$ (0.1 mM) in an aqueous medium using DMF as cosolvent at 20% in the case of DHP, Ph-DHP, nifedipine and amlodipine derivatives, and at 1% in the case of N-DHP (Fig. 1a). All the derivatives assayed reduced the gold salt in several degrees and generated AuNPs in one-step process, which was visualized by characteristic color changes and confirmed by spectroscopic and microscopic techniques. No AuNP formation was evidenced when experiments were performed in the absence of the dihydropyridines under the same conditions. This observations indicates that in our case DMF does not produce AuNPs, as occurs in other syntheses [46,47].

When N-DHP was assayed (0.1–1.0 mM, at 1% of DMF) as a model of NADH-type dihydropyridines, several color changes of the reaction medium were observed very quickly after gold salt addition: from colorless to pink, purple, blue and finally gray, in less than 20 s. This phenomenon was related to the very fast reduction of Au^{+3}, the generation of AuNPs and their rapid aggregation (data not shown). The destabilization was probably caused by the cation pyridinium generated *in situ* by oxidation of N-DHP (Fig. 1b), which could affect the electric double layer of the AuNPs leading to the rapid aggregation of the colloidal system. In this sense, some authors have reported that gold nanostructures could be pseudo-stabilized by chloride ions in absence of strong stabilizing agents, due to the halide ions could adsorbed on the gold particles giving them a negative surface charge [48–50]. In our case, probably the cation pyridinium produced *in situ* could interact with the chloride ions causing multiple electrostatic bridging, resulting in an irreversible agglomeration of the colloidal system. In contrast, when Hantzsch-type 1,4-dihydropyridines, such as Ph-DHP, nifedipine and amlodipine, were studied (0.15 mM, at 20% of DMF) the AuNPs generation was slower (5–30 min) and the colloidal system showed increased stability (data not shown). The lower rate of AuNPs formation using these derivatives compared to N-DHP is consistent with the electron-withdrawing effect of the substituents in position 4 that decreases the reducing capacity of the dihydropyridine nucleus [39–41], which is discussed below. Moreover, the major stability of the system is proposed to be related to the oxidation product generated in these cases, which corresponded to a neutral pyridine derivative (Fig. 1c) and therefore the surface charge and the electric double layer related with the chloride ions could be less affected. By spectrophotometry, the AuNPs produced using Ph-DHP showed a broad plasmonic band with a maximum around 550 nm, while nifedipine and amlodipine gave wider and less defined bands of lower intensity; and when the syntheses were performed using an excess of the 4-substituted 1,4-dihydropyridines (2.5 mM) at 25 °C only a slight broadening accompanied by a slight red-shifting of the spectrophotometric profile was evidenced (Fig. S2). However when the same syntheses were performed at 60 °C, the AuNPs formation was faster, providing a sharper plasmon band for Ph-DHP and nifedipine, whereas that for amlodipine continued to be broad and with low resolution (Fig. 2). In these conditions, nanostructures with a wide variety of shapes and sizes were observed by TEM analysis, such as spheres, rods, triangles, pentagons, hexagons and flowers mainly in the case of Ph-DHP and nifedipine, while the use of amlodipine yielded only amorphous particles (Fig. 2a, b and c). Based on these findings, each derivative showed a different behavior in the AuNPs formation, revealing that the structural characteristics of the dihydropyridines are closely related to the ease of formation of AuNPs, their morphology and stability.

Surprisingly, the simplest structural derivative DHP showed the most interesting results regarding to the homogeneity of shape and yield. We produced AuNPs with spherical or star-like shapes depending of the synthesis conditions, using only $HAuCl_4$, DHP, water, and DMF as cosolvent, at 25 °C, quickly and in one-step method.

To investigate the effect of the concentration of DHP on the AuNPs formation, different concentrations of the reducing agent were assayed while keeping the gold salt concentration constant

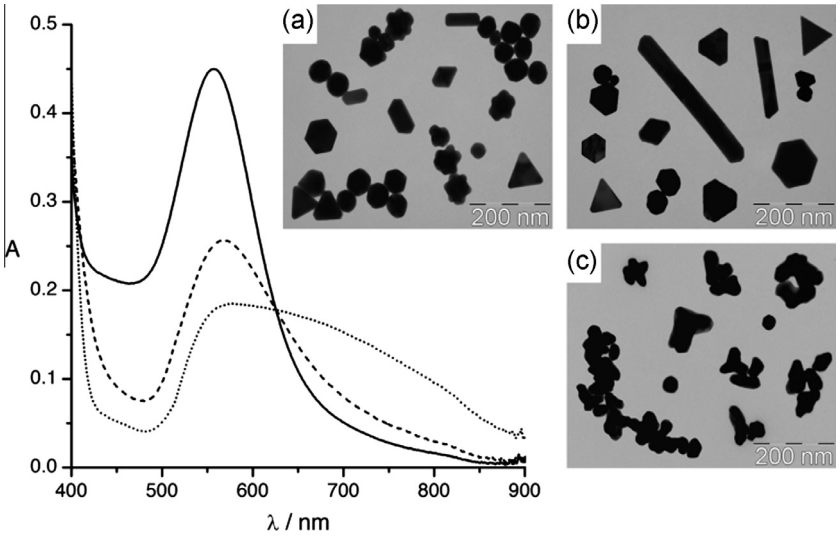

Fig. 2. Spectra of AuNPs obtained at 60 °C and 20% of DMF with a dihydropyridine:Au^{+3} ratio of 2.5:1, using: Ph-DHP (—), nifedipine (—) and amlodipine (····). Selection of representative AuNP shapes observed in several TEM analyses using: (a) Ph-DHP, (b) nifedipine and (c) amlodipine.

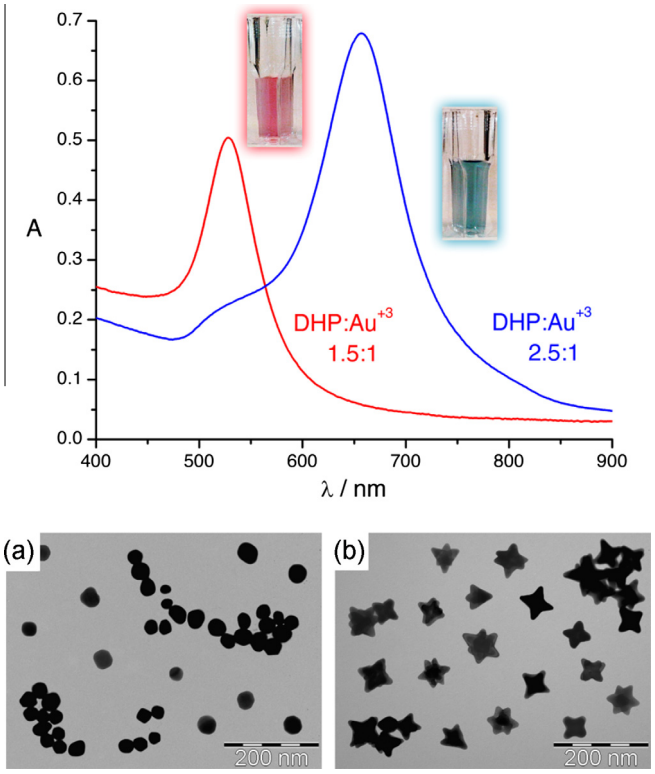

Fig. 3. Absorption spectra of AuNPs obtained at 25 °C and 20% of DMF at different ratios of DHP:Au^{+3}. TEM images of representative AuNPs obtained at ratios of: (a) 1.5:1 and (b) 2.5:1.

at 0.1 mM. Typical spectrophotometric profiles of the AuNPs obtained at low and high ratios of DHP:Au^{+3} are shown in Fig. 3. When low ratios were used (less than 1.5:1), the color of the reaction medium changed after addition of the gold salt, going from light yellow to pink within 40 s, and a sharp surface plasmon peak at 528 ± 5 nm (n = 6) was evidenced. When the synthesis was performed at a 1.5:1 ratio of DHP:Au^{+3}, all the particles observed by TEM were spherical with an average size of 43 ± 6 nm (Fig. 3a). In their colloidal state, these particles were stable for more than three months at 4 °C. Interestingly, when higher ratios were assayed (DHP:Au^{+3} 2.5:1), the color of the reaction medium turned turquoise in less than 1 min. These new particles exhibited a well-defined visible spectrum, with a strong surface plasmon peak at 651 ± 20 nm (n = 10) and a poorly defined shoulder around 530 nm, probably related with their longitudinal and transversal surface plasmon, respectively, which is in accordance with reports in the literature for branched AuNPs [11,22,51,52]. After carry out repeated synthesis of nanostructures produced at DHP:Au^{+3} 2.5:1 we observed reproducible plasmons, even changing the DMF supplier and different batches of the gold salt, which are presented in Supporting information (Fig. S3). Practically all the particles observed by TEM revealed a star-like morphology (over 96%), mostly with four or six tips, and no other branched shapes were detected (Fig. 3b). The average diameter of the nanostars obtained in three separate syntheses was 68 ± 11 nm, while the length of the tips was 18 ± 3 nm, as calculated by measuring at least 100 particles of each synthesis. In addition, this synthesis showed a practically complete conversion of initial Au^{+3} towards gold nanostructures of 94 ± 2%. On the other hand, at a DHP:Au^{+3} ratio of 3.5:1 the reaction medium undergoes different color changes, going from light yellow, pink, blue and finally purple-grey in a minor time than in previous cases, showing a gradual aggregation after some minutes. In this synthesis a broad plasmon of low intensity was obtained with two bands poorly defined around 580 and 800 nm, and particles without a well-defined shape were observed by TEM (Fig. S4). In summary, the proper formation of the well-defined nanostars was strongly influenced by the DHP concentration, and assaying intermediate conditions we can noted that its characteristic plasmon is only obtained by using at DHP:Au^{+3} ratio between 2:1 and 2.75:1, which showed a plasmon peak between 620 and 690 nm, respectively (Fig. S5). Furthermore, when the synthesis was performed at higher temperature (60 °C) by using the DHP:Au^{+3} ratio of 2.5:1, we only observed that the nanostars particles formation was faster than 25 °C, changing the color of the reaction medium from light yellow to turquoise in less than 15 s, and no significant difference was evidenced regarding to the plasmon, shape and homogeneity of the particles obtained (Fig. S6). Taking into account the above, we propose that in the case of the nanostar synthesis, the temperature mainly influences the rate of the process and not in the morphology of the particles obtained.

To elucidate why each dihydropyridine showed a different behavior in the obtention of the nanostructures (morphology and reaction rate), we performed electrochemical measurements to determinate their oxidation potential under the same experimental conditions used for the nanoparticle synthesis. After studying the Hantzsch dihydropyridines (Fig. S7a), we observed that the derivatives substituted in position 4 with aromatic groups (Ph-DHP, nifedipine and amlodipine) have a high oxidation potential (836, 920 and 958 mV, respectively), unlike that found for DHP (364 mV). The high potential showed by the 4-substituted dihydropyridines is related with the electron-withdrawing effect of the aromatic group, which decreases the reducing power of the dihydropyridine nucleus [39–41]. Thus, we observed that the oxidation potential of the dihydropyridines would be related to the facility of forming gold nanoparticles by Au^{+3} reduction, more specifically in the rate formation, morphology and homogeneity of the nanostructures obtained. In this sense, DHP presented the lower oxidation potential and showed a rapid formation of highly homogeneous nanostructures, unlike what was observed for the other derivatives (Ph-DHP, amlodipine and nifedipine), which showed a high oxidation potential and low rates of AuNPs formation, producing nanostructures of several shapes and sizes. In addition, the high oxidation potential (lower reducing power) of amlodipine and nifedipine also would be related with the low intensity of the plasmon bands that showed their colloids, which is probably due to an incomplete reduction of gold salt for forming Au^0 and gold nanostructures.

In order to evaluate the effect of DMF percentage in the gold nanostars formation, we carried out the synthesis at a constant ratio of DHP:Au^{+3} (2.5:1) assaying low DMF percentages (10% and 15%) and high DMF percentages (25%, 30%, 40%, 60%). When low DMF percentages were used, the reduction of the gold salt and nanoparticles formation was faster than with DMF at 20%, observing a complete color change in the reaction medium around 25 s and 45 s (at 10% and 15% of DMF, respectively). In both cases, well-defined plasmons with only a band around 520 nm were observed by spectrophotometry, which are typically described for pseudo-spherical particles. On the other hand, when high DMF percentages were assayed, we observed a dramatic increase in the time formation of nanoparticles, obtaining slow color changes in the reaction medium (from light yellow to light pink) from around 2 min to 20 min (at 25% and 60% of DMF, respectively). In these cases, plasmons of low intensity and resolution with a band around 520–540 nm were obtained, and no well-defined branched particles were observed by TEM. Typical plasmons and TEM images at different DMF percentages are presented in Fig. S8. Notably gold nanostars are produced at percentages of DMF close to 20%, and when lower or higher percentages than 20% are used pseudospherical and amorphous particles tend to be produced.

Taking into account that the organic solvent/water ratio could influence the redox process related to AuNPs formation, we studied the electrochemical behavior of DHP at different DMF percentages. In these experiments we observed an increase in the oxidation potential of DHP, from 358 mV to 470 mV, as increased the DMF percentage in the medium, from 10% to 60%, respectively (Fig. S7b). The increment in the oxidation potential would be related with a decrease in the reducing power of the dihydropyridine nucleus that, in our case, would hinder the reduction process of the gold salt to produce nanoparticles. A similar effect of the organic solvent/water ratio in the oxidation potential of others dihydropyridines also has been reported in literature [40]. Thus, the DMF could be modulating the electrochemical potential of the dihydropyridines and consequently affecting the reduction rate of the Au^{+3} leading to changes in the final morphology of the particles. Furthermore, it is important to note that the percentage of DMF can modify the viscosity of the reaction medium and therefore could affect the diffusion process related to the gold nucleation and the crystal growth. In this sense, significant changes in the viscosity of the medium have been reported by other authors when different mixtures of DMF/water were assayed, observing an increase in almost three times when the mole fraction of DMF was around 0.2 ($\eta_{0.1} = 2.062$, $\eta_{0.2} = 2.782$, $\eta_{0.3} = 2.954$; $\eta_{H2O} = 1.026$, $\eta_{DMF} = 0.864$ mPa × s) [53]. The above considerations allows us to propose that the DMF could have a critical role in the control of the rate formation and final morphology of the particles, exerting a modulatory effect in the formation process of the nanostructures mainly on two levels: regulating the redox potential of DHP and the viscosity of the reaction medium. Thereby, at low percentages of DMF the DHP derivative have a high reducing power and the reaction medium have a low viscosity, which probably produces a rapid Au^{+3} reduction acompained of rapid gold nucleation and crystal growth into pseudospherical shape; in the contrast at high percentages of DMF the DHP derivatives decreases its reducing power slowing down the Au^{+3} reduction, acompained of a high viscosity of the medium, which would hinder an adequate nucleation and crystal growth into star-like shape. The above allow us to propose that although DHP is the redox agent in this synthesis, the presence of the cosolvent in the reaction medium have an important role in modulating the process of the gold particles formation, and therefore their amount and physicochemical characteristics can modify the rate reaction and the final shape of the particles.

With the purpose of to evaluate whether the oxidized DHP derivative (pyridine type), produced *in situ* upon reduction of Au^{+3}, is the main responsible in the formation of the branched AuNPs, we carried out experiments adding the pyridine compound (Pyr) into the synthesis medium. To perform this assay we took into account three main considerations. First, theoretically only 1.5 equivalents of DHP are required to reduce completely the Au^{+3} to Au^0; second, only spherical particles were obtained when the synthesis was carried out at DHP:Au^{+3} ratio of 1.5:1; and third, the star-like nanoparticles were produced at ratios of DHP:Au^{+3} around 2.5:1. Thus, whether the Pyr derivative is the main responsible for the generation of nanoparticles with the star-like shape, this type of branched particles (and not spherical) should be obtained when the Pyr compound is added to the synthesis that in normal conditions produces nanospheres. In this case, using a constant DHP:Au^{+3} ratio (1.5:1), we added into the reaction medium different ratios of Pyr:Au^{+3}, from 0.1:1 to 4.5:1, but surprisingly in any proportion assayed we observed the characteristic spectral profile of the star-like gold nanoparticles obtained at a DHP:Au^{+3} ratio of 2.5:1 (Fig. 4). In absence of Pyr we obtained spherical particles with its typical plasmon around 530 nm, but as we increase the Pyr:Au^{+3} ratio we observed a broadening of the plasmon band and a slight shift of its maximum absorbance towards higher wavelengths, which is usually related to an increase in diversity in shape and size of the nanoparticles produced. By TEM analysis we observed particles of different sizes and shapes, mainly pseudo-spherical, polygonal and rod-like nanostructures (Fig. 4a). Although no particle with star-like shape was obtained with the addition of the Pyr derivative into the reaction medium, we observed that this compound modify the final shape of the nanostructures inducing an asymmetric growth in some particles, which could be due to a preferential affinity for certain faces of the growing gold crystal [54]. These results allow us to propose that the Pyr derivative, generated *in situ*, would not be the solely factor responsible for the production of star-like gold nanostructures, and that probably the formation process and colloidal stability involve a more complex mechanism also influenced by presence of the other species in the reaction medium, such as DMF and the DHP in excess.

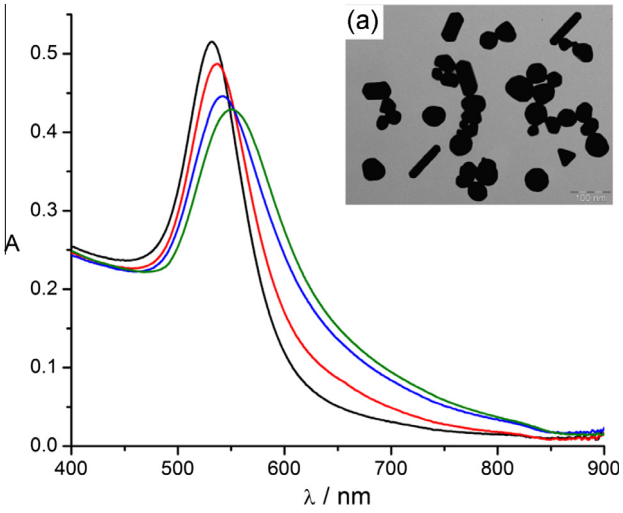

Fig. 4. Effect of Pyr on the plasmon of the AuNPs synthesized at a constant ratio of DHP:Au^{+3} (1.5:1; $HAuCl_4$ 0.1 mM), 25 °C and 20% of DMF. Ratios of Pyr:Au^{+3} assayed: 0:1 (—), 1.5:1 (—), 3:1 (—) and 4.5:1 (—). a) TEM images of AuNPs obtained at Pyr:Au^{+3} ratio of 3:1.

To better understand the formation process of the nanostars, we performed spectrophotometric measurements in real time (Fig. 5). We observed that after addition of $HAuCl_4$ to the reaction medium there is a rapid oxidation of DHP (decrease of band at 376 nm) to their respective Pyr derivative (increase of band at 274 nm), which is in accordance with the reduction of the Au^{+3} and generation of gold particles. Furthermore, a plasmonic band at 535 nm appears around 15–20 s of reaction, and a new plasmonic band at higher wavelength around 660 nm was observed from 25 to 30 s of reaction. Taking into account that the oxidation of DHP to Pyr derivative involve the transfer of two electrons (Fig. 1c) and that the reduction of Au^{+3} to Au^0 involve three electrons, is probably that in the formation process of gold nanostars first occur the reduction of one equivalent of Au^{+3} to Au^{+1} promoted by oxidation of one equivalent of DHP to Pyr, and then two equivalents of Au^{+1} are reduced subsequently to Au^0 by other equivalent of DHP, with the spontaneous formation of pseudo-spherical gold nuclei, which is in accordance to reported by other authors for generation of branched gold nanoparticles [55]. In addition, the same nuclei formed *in situ* also could catalyze the reduction to Au^0, in an similar manner to that observed for the seed-mediated approach [56]. Subsequently these nuclei continue to grow anisotropically until they achieve a star-like shape, due to the preferential deposition of gold atoms on certain faces of the gold crystal, probably controlled by the presence of DHP in excess, Pyr generated *in situ* and DMF in the medium.

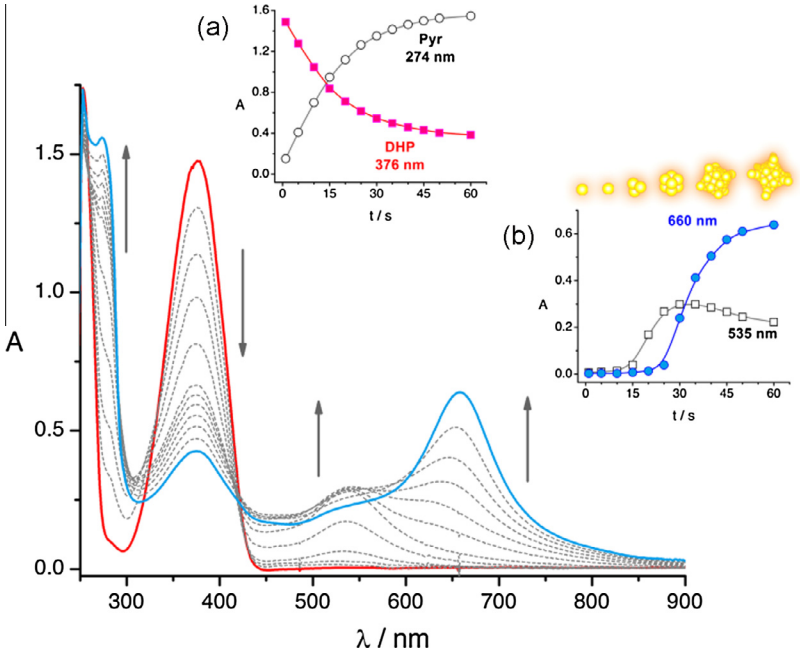

Fig. 5. Spectrophotometry in real time of the synthesis of star-like AuNPs showing the UV–vis changes in the first 60 s. Changes in the absorbance of (a) DHP/Pyr and (b) AuNPs formation with time.

To obtain more information concerning the structure of the nanostars, we performed a tomographic 3D reconstruction. A tilt image series ranging from +60° to −60° was acquired by STEM using a high angle annular dark field detector (HAADF) (Fig. 6). The 3D reconstruction is presented as a video file in the SI. Analysis of the reconstructed volume from different viewpoints reveals that the two particles had different shape: the larger one had eight vertexes, arranged in a cubic structure, while the small one had four vertexes, arranged in a tetrahedron. Therefore, the particles that we observe as stars with six tips are probably cubes with elongated vertexes, while the stars with four tips could correspond to a tetrahedron with elongated vertexes. However, it is important to take into account that, from other perspective, the same elongated cubic structure could be seen as a star with four tips. This approach is consistent with the information obtained by AFM, where practically all the particles visualized were star-like AuNPs with four tips projected on the plane (Fig. S9). Therefore, probably the nanostars with six and four tips are actually the same type of particle (based in a cubic structure with elongated vertexes) but viewed from a different perspective.

Furthermore, the HR-TEM images and the SAED pattern evidenced the presence of atomic planes related to a face-centered cubic (fcc) lattice specific to gold. The spacing for adjacent lattice planes of the most of the nanostars analyzed was 2.36 Å, which corresponds to a (111) plane and suggests that the particles were single crystals in most cases (Fig. 7). When the particles were observed perpendicular to one face, the planes parallel to the surface corresponded to (001) planes, as well as the zone axis, also corresponding to a (001) direction. In addition, given that the nanostars with six and four tips are in fact the same type of particle, the results from electron diffraction and HR-TEM can be interpreted as the faces of the cubes in the (001) directions and the tips correspond to growth in the (111) directions, which is in agreement with the observed for other branched gold nanoparticles [17–20]. Probably the preferential growth of the nanostars in the (111) lattice plane could be attributable mainly to the DHP

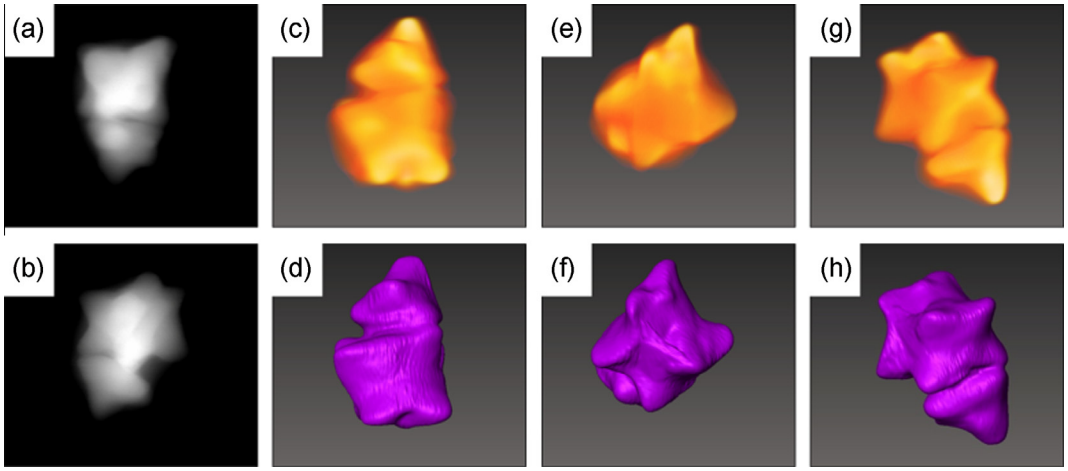

Fig. 6. HAADF projections of nanostars captured at different angles that highlight their structures (a, b); direct visualizations of the reconstructed volume (c, e, g); surface visualization after the segmentation of the volume (d, f, h).

molecules present in excess in the solution and also to the Pyr molecules generated *in situ*, which could be physisorbed on the (0 0 1) plane of the gold crystal in the early stages of particle formation, producing an orientation effect and facilitating the star-like morphology. The above is based on the fact that the nanostars are produced only when an excess of DHP is present, and that the incorporation of Pyr to the reaction medium affected the final shape of the nanostructures generated at a 1.5:1 ratio of DHP:Au^{+3} but not produced star-like gold nanoparticles. In this sense, the preferential formation of gold nanostars was strongly influenced by the structural characteristics of the dihydropyridines and the synthesis conditions, since these were obtained homogeneously and in high yield only when an excess of DHP was used. This suggests to us that DHP would have an important role as a growth directing agent of the gold crystal and as a stabilizing agent of the final structure. When dihydropyridines with aromatic substituents in position 4 were studied, the preferential formation of nanostars was not observed even when the synthesis was performed at high temperatures. Based on these observations, it is possible to propose that the structural changes in this position affect the adequate physisorption of dihydropyridine/pyridine molecules on the (0 0 1) plane of the gold crystal, and thus the preferential deposition of gold atoms in the (1 1 1) plane, and that probably the exposition and orientation of the carbonyl groups of the side chains are also involved in this process. Furthermore, the preferential growth was also influenced by the DMF percentage in the reaction medium, which exerted a critical role in the formation rate of the AuNPs and consequently in their final morphology, obtaining star-like structures only around 20% of DMF, as was described above in the experiment related with the effect of DMF in nanostars formation.

According to the results discussed above, we could propose a mechanism for gold nanostars formation based in the reduction of Au^{+3} to Au^{0} by DHP, either in one step or more probably via Au^{+1} intermediate. After, when the solution is supersatured with Au^{0} species, which are thermodynamically unstable, they spontaneously aggregate to form gold nuclei, and the remaining dissolved gold atoms bind to the nucleation sites to begin the crystal growth. The anisotropic growth is promoted by the excess of DHP and the presence of their oxidized derivative (Pyr). Furthermore, this process is strongly influenced by the DMF as cosolvent, which directly affects the oxidation potential of the reducing agent and the viscosity of the reaction medium, affecting the diffusion of the reactants (gold atoms, DHP and Pyr) and consequently the asymmetric growth.

Studying the stability of star-like AuNPs for one week at room temperature, we observed significant changes in the color of the solution (from turquoise to pink) and in the spectrophotometric profile (Fig. 8). The particles of the final solution were pseudo-spherical, as determined by TEM (Fig. 8a) and SEM (Fig. S10). The natural transformation of branched AuNPs into pseudo-spheres has been reported previously [7,25,26]. Given the above observations, and to investigate how easy it is to modify the surface of the nanostars obtained, we assayed their stabilization and functionalization with biomolecules, specifically by using two cysteine-containing peptides: one of low molecular weight (LMW) and other of high molecular weight (HMW) (Fig. S1).

When the LMW peptide was used, a bathochromic shift of the plasmon band from 640 to 646 nm was observed after 5 min of peptide addition, and the band stabilized at 648 nm after 48 h (Fig. 8), which is in agreement with other studies that used thiolated molecules to functionalize AuNPs [3,7]. A similar spectral shift of 15 nm was observed at 48 h when the HMW peptide was used. TEM images corroborated that the nanostars functionalized with LMW or HMW peptides keep their shape and size, with no evolution to spheres after 48 h (Fig. 8b). Analyzing these particles by dynamic light scattering (DLS), we observed that the unfunctionalized nanostars showed an hydrodynamic diameter of 97 ± 2 nm, which increased to 106 ± 2 nm and 118 ± 2 nm after functionalization with the LMW and HMW peptides, respectively. Typical correlograms and intensity distribution of the samples are showed in Fig. S11. These size increments were in accordance with the presence of molecules grafted on the nanostructures. Remarkably the hydrodynamic diameter increment was higher when the molecular weight of the functionalizing molecule was higher (e.g. the larger peptide (HMW) showed the biggest hydrodynamic diameter). Furthermore, the unfunctionalized particles showed a negative Z potential of −25 ± 1 mV, which practically remain unchanged after their conjugation with the peptides of LMW (−27 ± 2 mV) and HMW (−28 ± 1 mV). Furthermore, in order to evidence the peptides grafted on the AuNPs surface, we performed a negative staining of the samples using uranyl acetate as contrast agent, which is frequently used for visualizing biological samples by electron microscopy due to its ability to be included in the organic material and to provide electrodense contrast areas [57]. TEM analysis revealed a characteristic edge on the surface of the nanomaterial when the HMW peptide was used, confirming its conjugation to the nanostars (Fig. 8c).

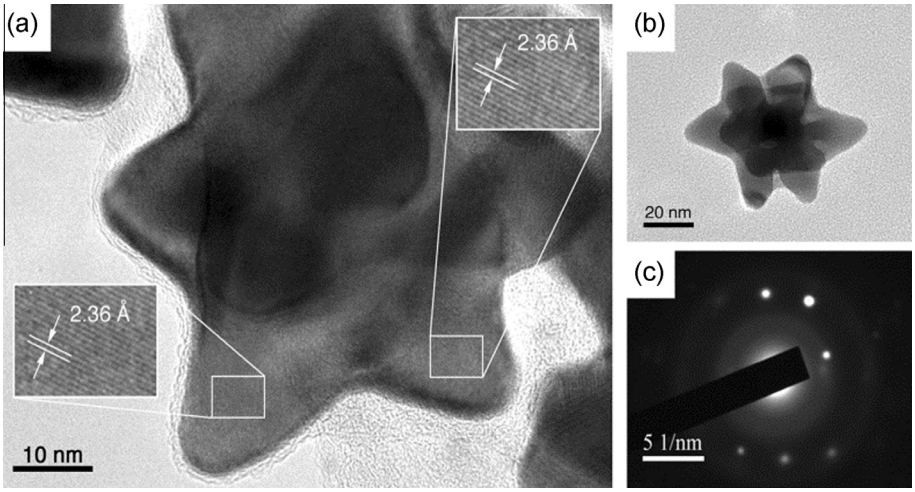

Fig. 7. (a) HR-TEM image of a nanostar showing the d-spacing that corresponds to the (1 1 1) plane. (b) Image and (c) electron diffraction pattern of another gold nanostar along one vertex.

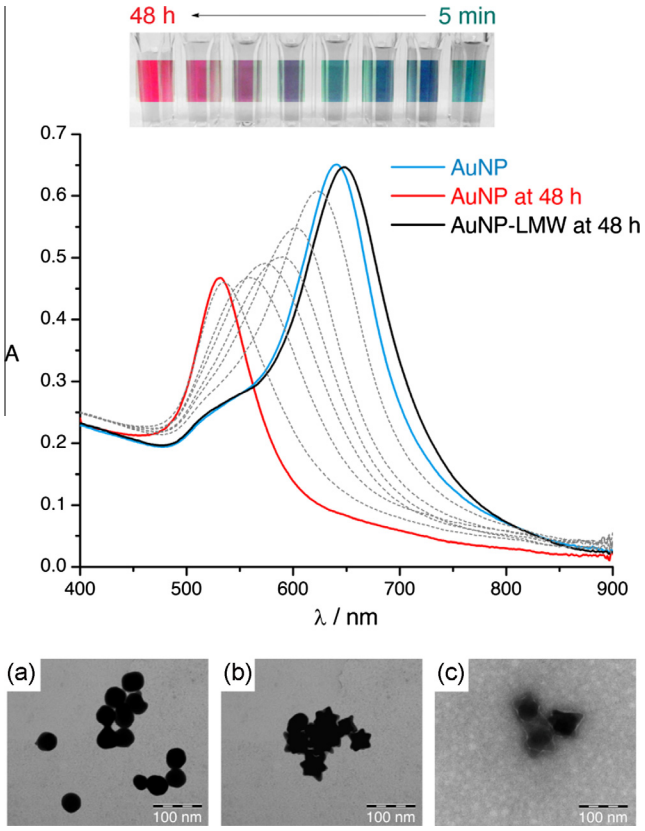

Fig. 8. Visual and spectral changes observed over time of unfunctionalized star-like AuNPs and functionalized AuNPs with LMW peptide. TEM images after 48 h of: (a) unfunctionalized AuNPs, (b) LMW-AuNPs, (c) HMW-AuNPs staining with uranyl acetate.

In addition, the functionalized AuNPs with LMW and HMW peptides were stable in their colloidal state and keep their morphology for more than six months when stored at 4 °C. To evaluate the chemical and biological potential applications we studied spectrophotometrically the stability of the nanostars in different interesting conditions for 48 h at room temperature and light exposure, such as centrifugation, phosphate buffer saline pH 7.4 (PBS), 0.9% NaCl (saline solution), 0.1 M HCl and 0.1 M NaOH. In general terms, the functionalized nanostars showed a higher stability than unfunctionalized particles in all assayed conditions. The unfunctionalized nanostars were unstabilized quickly in few minutes when they were in contact with PBS, saline solution, acid or basic medium, which was evidenced by changes in the shape and intensity of their characteristic plasmon and by the aggregation of the colloidal solution (Fig. S12a). These particles showed a slower change in their plasmon after they were centrifugated and resuspended in the same clean medium, revealing that they were slightly stable to this process, although finally they also aggregated in less than 24 h. On the other hand, the functionalized nanostars with LMW and HMW peptides showed a high stability after a centrifugation and resuspension process, with a plasmon band that remained unchanged even after 7 days. However, when PBS, saline solution, acid and basic conditions were assayed, the nanostars functionalized with LMW peptide showed a loss of the characteristic plasmon band around 6 h, which was related to an irreversible colloidal aggregation indicating that this peptide not increased significantly the stability of the particles in these conditions (Fig. S12b). The unstability in PBS can be attributed to the high ionic strength present that reduces the Debye length and consequently the double layer. Surprisingly, when the HMW peptide was used only a slight hypochromic effect in the plasmon band was observed after 6 h in PBS and basic medium, whereas in saline solution and acid medium showed faster changes (Fig. S12c), revealing that these functionalized nanostructures are more stable than unfunctionalized particles and the modified with LMW. It is important to note that the increased stability of the HMW-nanostars respect to LMW-nanostars, in all conditions assayed, is in accordance with the size of each peptide and the steric effect that they can produce to stabilize the colloid. The unstability in acidic condition would be related to a low ionization of the acid groups present in each peptidic structure due to the pH of the medium (the pI of the peptides are 5.6 and 7.2 for LMW and HMW, respectively), producing a decrease in the surface charge of the nanostructures and consequently their colloidal aggregation, which would not occur in the other assayed conditions. Therefore, here we demonstrate that the star-like AuNPs synthesized can be easily modified with peptides improving their stability and rendering them potentially useful for chemical and biological applications.

4. Conclusions

Here we describe a novel one-step method for the preparation of different gold nanostructures using dihydropyridines as reducing agents. The use of dihydropyridines with different substituent patterns produced AuNPs of diverse shapes and sizes, which involves possibly a manifold mechanism strongly influenced by the structural features and reducing power of these molecules. Using the DHP derivative, a dihydropyridine structurally simple, we achieve to control the final shape of the gold nanostructures producing selectively nanospheres or nanostars highly homogeneous in shape (over 96% in both cases) only by changing the amount of reducing agent in the reaction medium. The well-defined gold nanostars were synthesized quickly in high yield at 25 °C, and presented an average size of 68 nm with mostly four or six tips, which had an average length of 18.2 nm. These particles showed a strong absorption spectra with two bands in the visible region due to transverse and longitudinal plasmon resonances of the tips. The nanostars grew preferentially in the (111) plane, probably by an orientation effect of dihydropyridine/pyridine molecules physisorbed on the (001) plane of the gold crystal. Furthermore, these nanostructures were conveniently stabilized and functionalized by conjugation to thiolated peptidic biomolecules remaining stable for more than six months in their colloidal state, which can then be further used for chemical and biomedical applications. Therefore, this new approach using dihydropyridines as reducing agents represent a straightforward synthesis of gold nanostructures with controlled shape, without the use of surfactant and feasible for use in future applications.

Supporting information

Supplementary data associated with results and a video of the 3D reconstruction of the gold nanostars are provided as supporting information (SI) in the online version.

Acknowledgment

This study was funded by the CICYT (CTQ2012-30930), the Generalitat de Catalunya (2009SGR1024), IRB Barcelona, Spain, AECID, FONDECYT 1130425, MECESUP–UCH 0811 and FONDAP 15130011. Claudio Zapata-Urzúa and Magdalena Pérez-Ortiz are grateful to CONICYT for the PhD fellowships and to Vicerectory of Academic Issues (University of Chile) for the research stay fellowships.

Appendix A. Supplementary material

Supplementary data associated with this article can be found, in the online version, at http://dx.doi.org/10.1016/j.jcis.2015.04.050.

References

[1] B. Pelaz, P. del Pino, in: J.M. de la Fuente and V. Grazu, (Eds.), Frontiers of Nanoscience, Elsevier, 2012, vol. 4, ch. 1, pp. 3–33.
[2] D. Pissuwan, T. Niidome, M.B. Cortie, J. Controlled Release 149 (2011) 65–71.
[3] I. Olmedo, E. Araya, F. Sanz, E. Medina, J. Arbiol, P. Toledo, A. Álvarez-Lueje, E. Giralt, M.J. Kogan, Bioconjugate Chem. 19 (2008) 1154–1163.
[4] E. Hao, R.C. Bailey, G.C. Schatz, J.T. Hupp, S. Li, Nano Lett. 4 (2004) 327–330.
[5] J. Xie, Q. Zhang, J.Y. Lee, D.I. Wang, ACS Nano 2 (2008) 2473–2480.
[6] L.F. Zhang, S.L. Zhong, A.W. Xu, Angew. Chem. Int. Ed. 52 (2013) 645–649.
[7] B. Van de Broek, F. Frederix, K. Bonroy, H. Jans, K. Jans, G. Borghs, G. Maes, Nanotechnology 22 (2011) 15601–15610.
[8] H. Yuan, A.M. Fales, T. Vo-Dinh, J. Am. Chem. Soc. 134 (2012) 11358–11361.
[9] A. Mohanty, N. Garg, R. Jin, Angew. Chem. Int. Ed. 49 (2010) 4962–4966.
[10] W. Wang, Y. Pang, J. Yan, G. Wang, H. Suo, C. Zhao, S. Xing, Gold Bull. 45 (2012) 91–98.
[11] C.L. Nehl, H. Liao, J.H. Hafner, Nano Lett. 6 (2006) 683–688.
[12] L. Sironi, S. Freddi, M. Caccia, P. Pozzi, L. Rossetti, P. Pallavicini, A. Donà, E. Cabrini, M. Gualtieri, I. Rivolta, A. Panariti, L. D'Alfonso, M. Collini, G. Chirico, J. Phys. Chem. C 116 (2012) 18407–18418.
[13] B. Van de Broek, N. Devoogdt, A. D'Hollander, H. Gijs, K. Jans, L. Lagae, S. Muyldermans, G. Maes, G. Borghs, ACS Nano 5 (2011) 4319–4328.
[14] P. Pallavicini, A. Donà, A. Taglietti, P. Minzioni, M. Patrini, G. Dacarro, G. Chirico, L. Sironi, N. Bloise, L. Visai, L. Scarabelli, Chem. Commun. 50 (2014) 1969–1971.
[15] A. Guerrero-Martínez, S. Barbosa, I. Pastoriza-Santos, L.M. Liz-Marzán, Curr. Opin. Colloid Interface Sci. 16 (2011) 118–127.
[16] B. Pelaz, V. Grazu, A. Ibarra, C. Magen, P. del Pino, J.M. de la Fuente, Langmuir 28 (2012) 8965–8970.
[17] W. Moukarzel, J. Fitremann, J.D. Marty, Nanoscale 3 (2011) 3285–3290.
[18] J. Xie, J.Y. Lee, D.I. Wang, Chem. Mater. 19 (2007) 2823–2830.
[19] L. Li, J. Weng, Nanotechnology 21 (2010) 305603–305612.
[20] J. Li, J. Wu, X. Zhang, Y. Liu, D. Zhou, H. Sun, H. Zhang, B. Yang, J. Phys. Chem. C 115 (2011) 3630–3637.
[21] Y. Lee, T.G. Park, Langmuir 27 (2011) 2965–2971.
[22] T. Ishizaka, A. Ishigaki, H. Kawanami, A. Suzuki, T.M. Suzuki, J. Colloid Interface Sci. 367 (2012) 135–138.
[23] S. Chen, Z.L. Wang, J. Ballato, S.H. Foulger, D.L. Carroll, J. Am. Chem. Soc. 125 (2003) 16186–16187.
[24] T.K. Sau, C.J. Murphy, J. Am. Chem. Soc. 126 (2004) 8648–8649.
[25] C.H. Kuo, M.H. Huang, Langmuir 21 (2005) 2012–2016.
[26] H.Y. Wu, M. Liu, M.H. Huang, J. Phys. Chem. B 110 (2006) 19291–19294.
[27] L. Vigderman, E.R. Zubarev, Langmuir 28 (2012) 9034–9040.
[28] H.M. Chen, R. Liu, D. Tsai, Cryst. Growth Des. 9 (2009) 2079–2087.
[29] W. Ahmed, E. Kooij, A. van Silfhout, B. Poelsema, Nanotechnology 21 (2010). 125605-12610.
[30] S. Barbosa, A. Agrawal, L. Rodríguez-Lorenzo, I. Pastoriza-Santos, R.A. Alvarez-Puebla, A. Kornowski, H. Weller, L.M. Liz-Marzán, Langmuir 26 (2010) 14943–14950.
[31] M.L. Personick, C.A. Mirkin, J. Am. Chem. Soc. 135 (2013) 18238–18247.
[32] C. Grabinski, N. Schaeublin, A. Wijaya, H. D'Couto, S.H. Baxamusa, K. Hamad-Schifferli, S.M. Hussain, ACS Nano 5 (2011) 2870–2879.
[33] P. Senthil-Kumar, I. Pastoriza-Santos, B. Rodríguez-González, F.J. García de Abajo, L.M. Liz-Marzán, Nanotechnology 19 (2008) 15606–15612.
[34] P. Pallavicini, G. Chirico, M. Collini, G. Dacarro, A. Donà, L. D'Alfonso, A. Falqui, Y. Díaz-Fernández, S. Freddi, B. Garofalo, A. Genovese, L. Sironi, A. Taglietti, Chem. Commun. 47 (2011) 1315–1317.
[35] H. Yuan, C.G. Khoury, H. Hwang, C.M. Wilson, G.A. Grant, T. Vo-Dinh, Nanotechnology 23 (2012) 75102–75117.
[36] P. Pallavicini, A. Donà, A. Casu, G. Chirico, M. Collini, G. Dacarro, A. Falqui, C. Milanese, L. Sironi, A. Taglietti, Chem. Commun. 49 (2013) 6265–6267.
[37] R. Lavilla, J. Chem. Soc., Perkin Trans. 1 (2002) 1141–1156.
[38] D. Richter, H. Mayr, Angew. Chem. Int. Ed. 48 (2009) 1958–1961.
[39] R.H. Bockert, F.P. Guengerich, J. Med. Chem. 29 (1986) 1596–1603.
[40] L.J. Núñez-Vergara, J.C. Sturm, A. Álvarez-Lueje, C. Oléa-Azar, C. Sunkel, J.A. Squella, J. Electrochem. Soc. 146 (1999) 1478–1485.
[41] R. Salazar, P.A. Navarrete-Encina, C. Camargo, J.A. Squella, L.J. Núñez-Vergara, J. Electrochem. Soc. 155 (2008) 103–108.
[42] X.Q. Zhu, J.Y. Zhang, J.P. Cheng, J. Org. Chem. 71 (2006) 7007–7015.
[43] Y. Xiao, V. Pavlov, S. Levine, T. Niazov, G. Markovitch, I. Willner, Angew. Chem. Int. Ed. 43 (2004) 4519–4522.
[44] B. Shlyahovsky, E. Katz, Y. Xiao, V. Pavlov, I. Willner, Small 1 (2005) 213–216.
[45] International Standard ISO 22412:2008. Particle Size Analysis - Dynamic Light Scattering (DLS); Updates and extends ISO 13321:1996. Particle Size Analysis – Photon Correlation Spectroscopy.
[46] I. Pastoriza-Santos, L.M. Liz-Marzán, Langmuir 15 (1999) 948–951.
[47] Y. Chen, X. Gu, C.G. Nie, Z.Y. Jiang, Z.X. Xie, C.J. Lin, Chem. Commun. 33 (2005) 4181–4183.
[48] P.M. Shem, R. Sardar, J.S. Shumaker-Parry, J. Colloid Interface Sci. 426 (2014) 107–116.
[49] Z. Zhang, H. Li, F. Zhang, Y. Wu, Z. Guo, L. Zhou, J. Li, Langmuir 30 (2014) 2648–2659.
[50] S.E. Lohse, N.D. Burrows, L. Scarabelli, L.M. Liz-Marzán, C.J. Murphy, Chem. Mater. 26 (2014) 34–43.
[51] G. Maiorano, L. Rizzello, M.A. Malvindi, S.S. Shankar, L. Martiradonna, A. Falqui, R. Cingolani, P.P. Pompa, Nanoscale 3 (2011) 2227–2732.
[52] D. Senapati, A.K. Singh, P.C. Ray, Chem. Phys. Lett. 487 (2010) 88–91.
[53] J.M. Bernal-García, A. Guzmán-López, A. Cabrales-Torres, A. Estrada-Baltazar, G.A. Iglesias-Silva, J. Chem. Eng. Data 53 (2008) 1024–1027.
[54] P.R. Sajanlal, T.S. Sreeprasad, A.K. Samal, T. Pradeep, Nano Reviews 2 (2011) 5883–5945.
[55] S.N.K. Kamarudin, M.F. Mohamad, N. Dolmat, Int. J. Mater. Sci. (IJMSCI) 3 (2004) 72–77.
[56] J. Pérez-Juste, L.M. Liz-Marzán, S. Carnie, D.Y.C. Chan, P. Mulvaney, Adv. Funct. Mater. 14 (2004) 571–579.
[57] L. Hosta, M. Pla-Roca, J. Arbiol, C. López-Iglesias, J. Samitier, L.J. Cruz, M.J. Kogan, F. Albericio, Bioconjugate Chem. 20 (2009) 138–146.